AIAA SciTech Forum
12-16 January 2026, Orlando, FL
AIAA SCITECH 2026 Forum

10.2514/6.2026-1383

Lidar Maturation and Demonstration Activities in the Clean Aviation UP Wing Project

Nicolas Fezans*, Philippe Linsmayer†, Patrick Vrancken‡, Johann Thurn§, Daniel Kiehn¶ and Raoul-Amadeus Lorbeer‖
DLR (German Aerospace Center), Germany

Pierre Pichon**, Jonathan Pouillaude††, Thadek Ferrand‡‡ and David-Tomline Michel§§
ONERA (the French Aerospace Lab), France

Robert Tump¶¶ and Harald de Haan***
NLR (Netherlands Aerospace Centre), The Netherlands

This paper presents the current maturation and demonstration activities of forward-looking Doppler lidar sensors that allow measuring gusts ahead of the aircraft such that this information can be used for gust load alleviation controllers. With a limited lead time of the order of 0.5 seconds, the load alleviation performance of such controllers can be drastically improved, enabling wings that are lighter or have higher aspect ratios. For such an application, the sensor shall provide valid measurements even in the absence of aerosols. This requirement eliminates some of the most mature wind lidar technologies (e.g. coherent detection based on Mie scattering) and yields the need for mature direct-detection Doppler wind lidar in the ultraviolet wavelengths as they are able to exploit the Rayleigh scattering mechanism directly from the molecules of the air. Significant developments and demonstrations of these sensor technologies are currently being performed in the European Clean Aviation project "Ultra-Performance Wing" and are summarized in the paper. Experimental validations will be performed in 2026 at an alpine weather research station (about 2,650 m altitude) and in flight tests.

I. Introduction

The main levers for direct improvements in aircraft efficiency are reducing weight, reducing drag, improving the propulsion efficiency, or operating the aircraft in a more efficient manner. When assessing the climate-impact of aviation, indirect factors need to be considered such as current atmospheric conditions, when and where the flight takes place, time of day, and many other factors [1].

Whilst the other aspects are also important, the present work focuses on reducing the weight and the drag of the aircraft, or rather on enabling a better trade-off between weight and drag. It is being performed within a wing-oriented Clean Aviation project called "Ultra-Performance Wing" (UP Wing) in which a consortium of 26 partners across Europe investigate and maturate various innovative wing concepts and technologies. An overview of the entire UP Wing project can be found in [2] and in Fig. 1.

High-aspect-ratio wings (AR>14) can be a key contributor to significantly reducing the environmental footprint, aiming to reduce fuel burn thanks to reduced aerodynamic drag (reduction of induced drag), while the wing weight penalty should be minimized [2]. As schematically explained in the top-left corner of Fig. 1, increasing the wing aspect ratio typically yields overall performance improvements at moderate aspect ratios, but eventually a performance

*Scientific Advisor, Institute of Flight Systems, Braunschweig, Germany, Nicolas.Fezans@dlr.de, AIAA Associate Fellow.
†Research Assistant, Institute of Atmospherics Physics, Oberpfaffenhofen, Germany, Philippe.Linsmayer@dlr.de.
‡Research Scientist, Institute of Atmospherics Physics, Oberpfaffenhofen, Germany, Patrick.Vrancken@dlr.de.
§Research Scientist, Institute of Technical Physics, Stuttgart, Germany, Johann.Thurn@dlr.de.
¶Research Scientist, Institute of Flight Systems, Braunschweig, Germany, Daniel.Kiehn@dlr.de.
‖Research Scientist, Institute of Technical Physics, Stuttgart, Germany, Raoul.Lorbeer@dlr.de.
**Research Engineer, Optics and Associated Techniques Department (ONERA-DOTA), Palaiseau, France, Pierre.Pichon@onera.fr.
††Research Engineer, Optics and Associated Techniques Department (ONERA-DOTA), Palaiseau, France, Jonathan.Pouillaude@onera.fr.
‡‡Research Engineer, Optics and Associated Techniques Department (ONERA-DOTA), Palaiseau, France, Thadek.Ferrand@onera.fr.
§§Research Engineer, Optics and Associated Techniques Department (ONERA-DOTA), Palaiseau, France, David-Tomline.Michel@onera.fr.
¶¶Research Test Pilot / Flight Validation Pilot, Amsterdam, The Netherlands, Robert.Tump@nlr.nl.
***Senior Project Engineer / Flight Test Engineer / Flight Inspector, Amsterdam, The Netherlands, Harald.de.Haan@nlr.nl.

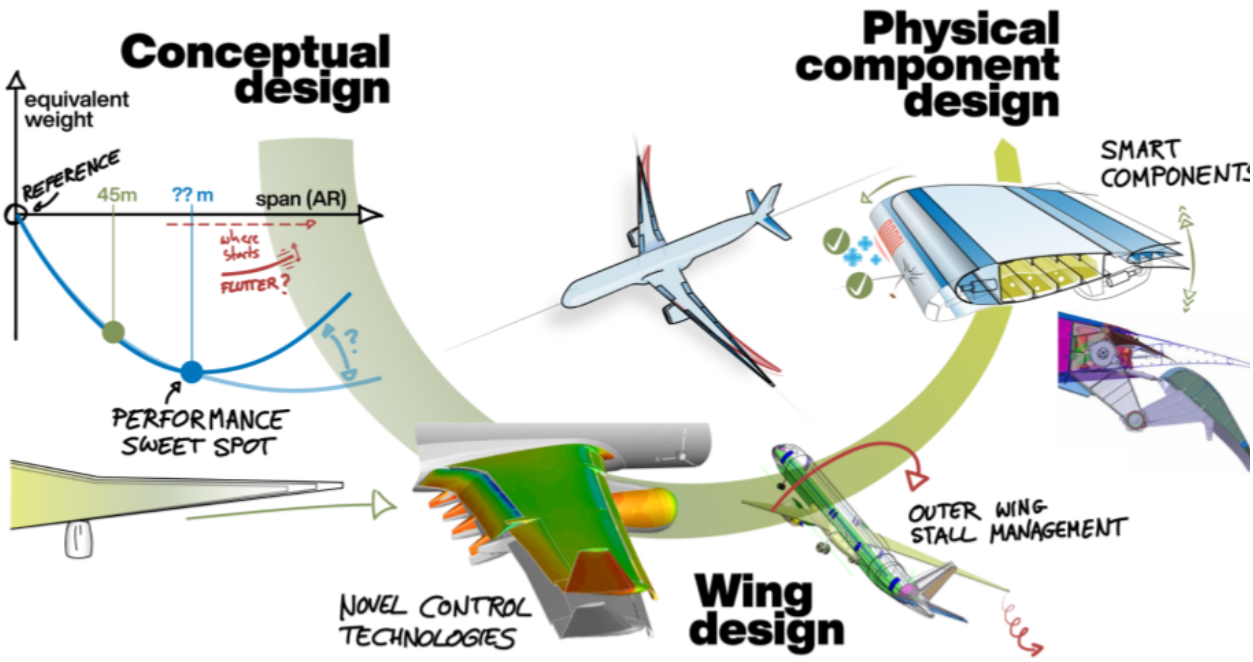

Fig. 1 Sketch of the UP Wing design process (cf. [2]).

sweet-spot is reached. Beyond the sweet-spot, a further increase in aspect ratio yields a decrease in the overall performance of the aircraft. The factor determining the sweet spot is usually either the structural loads (gust/turbulence or maneuver) or flutter / aeroelastic stability constraints. For smaller aspect ratios than at the sweet spot, the performance improvement due to the reduction of induced drag resulting from an increase in the aspect ratio dominates the performance deterioration due to the increase in structural weight resulting from increased loads and a more flutter-prone wing. At the sweet spot, both effects cancel each other out. Beyond the sweet spot, the weight penalty dominates the aerodynamic benefits.

This trade-off between weight and aerodynamic efficiency is always present, regardless of the technologies considered, but the introduction of more advanced technologies (e.g. more advanced materials) can allow simultaneous improvements on both weight and aerodynamic efficiency, compared to a configuration that is not using these technologies. In the present work, the new technologies considered are novel control technologies and in particular lidar-based gust load alleviation systems. Using Doppler wind lidar sensors that can detect the gusts and turbulence ahead of the aircraft, the gust load alleviation system can anticipate them (typically by about 0.5 s) and use the lead time to better alleviate their impact in terms of structural loads, fatigue, and also passenger safety and comfort. The developments and demonstrations presented in this paper are based on many years of prior studies and developments. Ref. [3] presents a good overview of 15–20 years of developments up to early 2020. This paper was written towards the end of the Clean Sky 2 programme in which some of these prior developments were made. One of the main conclusions of [3] was that to further progress in terms of technology maturation, new demonstrations and, in particular, in-flight demonstrations were needed. Two and a half years later, the Clean Aviation programme provided a good opportunity to pursue this work as part of the UP Wing project. This project started in January 2023 and will run until the end of 2026. Many of the new developments made since 2023 will be demonstrated in 2026.

The paper is structured in two main parts. First, Section II presents an overview of the technologies developed, then Section III presents the main on-going and forthcoming demonstrations.

II. Overview of the Main Technology Developments

This section presents the main technology developments that are undertaken in UP Wing on the lidar-based gust load alleviation (GLA) topic: the laser technologies in Section II.A, the beam steering in Section II.B, the detector technologies in Section II.C, the wind reconstruction algorithms in Section II.D, the control design methods in Section II.E, and finally the aircraft-level assessment in Section II.F.

A. Laser Technologies

Based on prior analyses made in previous projects (e.g., Clean Sky NACOR and the DLR-internal project COLOCAT*), DLR has built and is actively improving a UV laser compatible to DLR's Doppler spectrometric receiver prototype, cf. Section II.C. This laser is based on a MOPA (master oscillator power amplifier) concept starting with a SLM (single longitudinal mode, linewidth 125 MHz measured with a Fabry-Pérot interferometer) 1064 nm passively Q-switched micro-chip master oscillator (MO). The MO is followed by three amplifier stages and two LBO-crystals for harmonic generation of frequency-tripled pulses. The laser exceeds 6 W at 355 nm with 7 ns long pulses at 3 kHz repetition rate. This represents a solid basis and sufficient Rayleigh backscatter should be obtained for interferometric wind speed measurement at high altitude. After frequency tripling, the remaining fundamental and second harmonic beams are dumped. A remainder of the fundamental beam is coupled into a reference fiber such that the fundamental laser frequency can be monitored, while the UV beam is expanded to about 1 cm in diameter at the output window. The UV beam divergence is adjusted to match the requirements of DLR's field-widened fringe-imagine Michelson interferometer-based receiver.

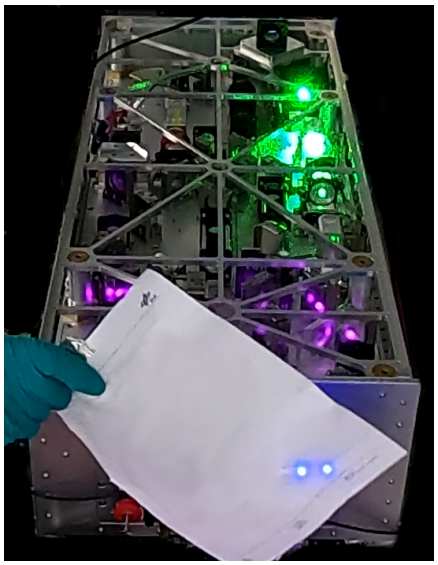

Fig. 2 DLR laser in final adjustment phase with low-power UV output projected on a sheet of paper.

The laser electronics consists of a Raspberry Pi 4 Compute Module on its IO Board, laser electronics for the pump diode and master oscillator, and an in-house developed control board. Functionality includes an interlock system, shutter and harmonic generation oven control, as well as pulse generation. More details on the design and implementation of this laser will be disclosed in future publications. The mechanical interface of the laser was developed to fit the existing flight test hardware used in previous experiments [4–6], which simplifies the integration and paperwork for the upcoming flight tests. The optical part is sealed in a dust-free environment to ensure the longevity of the optical components. The finished laser is shown in Fig. 2.

An alternative laser technology is also developed and investigated by ONERA: a frequency-tripled, pulsed 1030 nm hybrid fiber laser, i.e. with a possible boost free-space amplification stage and solid-state IR-UV† frequency conversion. Its specifications are also optimized for the combination with ONERA's development of a Doppler receiver based on a Quadri-channel Mach-Zehnder interferometer (QMZ), cf Section II.C. More precisely, thanks to a frequency comb adapted to the free spectral range of the QMZ, the pulse energy amounts to 350 µJ at the output of the fiber system at 40 kHz repetition rate (14 W average power). The resulting output beam is then amplified up to 36 W average power in a Yb:YAG slab that enable an efficient frequency conversion from the native IR to UV. Finally, the laser emits 9.2 W at 343 nm for 25 ns pulses at 40 kHz repetition rate. The design of the laser is now validated and ONERA is currently working on the airborne integration which requires high mechanical stability, especially for the free space frequency conversion. Figure 3 shows this laser during lab tests.

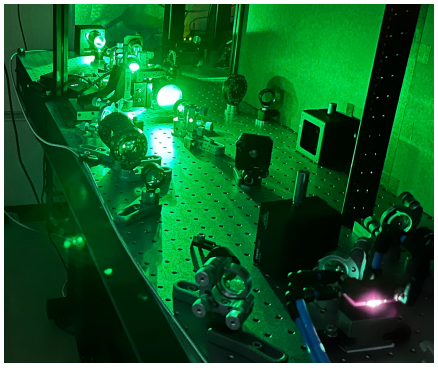

Fig. 3 Hybrid UV laser under test at ONERA.

*COLOCAT: Compact Optical sensors for LOad alleviation of Clear Air Turbulence.

†Infrared (IR) to ultraviolet (UV)

B. Beam Steering / Scanning / Addressing

Beam addressing is a key element for most wind lidars to probe a specific area of the atmosphere or to reconstruct the 3D wind by measuring several of its components. This latter case is the motivation for developing a beam addressing system within the UP Wing project. For load reduction, the wind perpendicular to the aircraft's path must be determined using a wind reconstruction algorithm (cf. section II.D) which requires measurements in multiple directions. To carry out the initial reconstruction tests, ONERA developed a turret composed of a set of three mirrors forming an assembly resembling a periscope (see Fig. 4) and addressing all directions of the half-space above the turret. In this instrument, two mirrors are motorized so that the desired angles can be addressed from the lidar control interface.

In parallel, a thorough literature review was conducted to determine the most suitable addressing methods for UP Wing. Currently, based on this study, two different addressing methods are being developed at DLR and ONERA, both based on static directions to be addressed in order to minimize complexity and in particular moving parts in future airborne demonstrations or the final application.

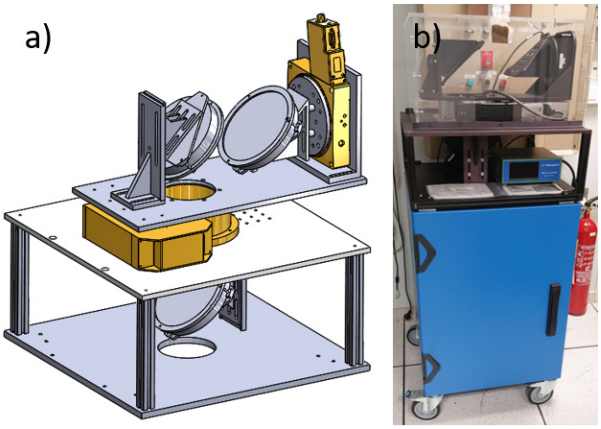

Fig. 4 Turret developed to perform first test of lidar scanning: a) CAD model with the main optical systems b) integrated on test hardware.

C. Detector/Receiver Technologies

The spectrometric receivers of direct-detection Doppler wind lidars are based on optical interferometry, by which the Doppler-shifted (by the relative wind) frequency of the backscattered light is analyzed and compared to the emitted one (hence the term "direct detection"). In a previous lidar sensor developed and demonstrated during the AWIATOR project, a Fabry-Pérot interferometer was used in imaging mode [7, 8]. The interferometer produces a circular pattern whose diameters are functions of the wavelength. The frequency analysis requires the measurement of this two-dimensional circular pattern and thus a two-dimensional detector is needed. In AWIATOR this was solved with a CCD (after amplification), and as many values as pixels must be processed, for example using a circle Hough transform, cf. [9]. This setup also engendered an analysis of a sole distance (i.e., some 350 m in front) to be measurable.

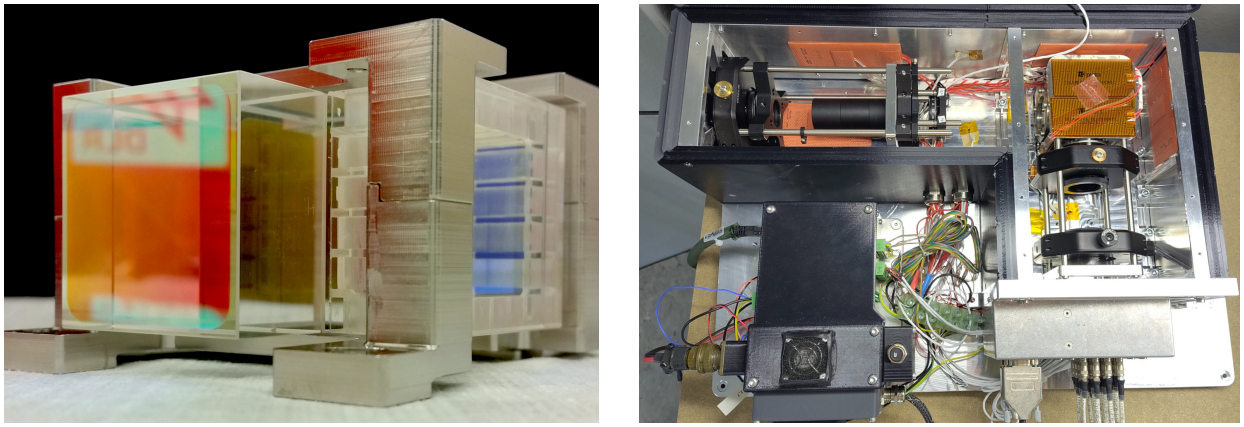

(a) DLR's field-widened fringe-imaging Michelson interferometer at the heart of the Doppler spectrometric receiver.

(b) The airborne demonstrator version of the Doppler spectrometric receiver based on the Michelson interferometer.

Fig. 5 Doppler spectrometric receiver based on the field-widened fringe-imaging Michelson interferometer.

With the aim of increasing the efficiency of the detection process, and the data processing, two alternative detector technologies are investigated [10] within the UP Wing project, both based on "two-path interferometers" as opposed to a multi-path interferometer (like Fabry-Pérot within AWIATOR). These allow, by implementing field-widening (FW), for

robustifying their response against angular deviations which can be induced by vibrations (e.g., due to turbulence). DLR has been studying and demonstrating [11–13] a setup based on a field-widened skewed Michelson interferometer Fig. 5a in fringe-imaging mode (FWFIMI) that, due to one of the mirrors being slightly skewed, produces a linear interference pattern. This is then imaged and compressed along one axis and subsequently detected on only a one-dimensional array of photomultiplier tubes (PMT). The spatial position of the fringe (i.e., its cosine-shaped amplitude distribution) on the detector then gives the frequency of both a part of the emitted laser pulse and of the backscattered light at a series of relevant distances (i.e., from 50 to 350 m with a range resolution of some meters) [14]. The setup developed for airborne demonstration on the NLR Cessna Citation II aircraft is depicted in Fig. 5b (with opened lid): The light to be analyzed is guided by an optical fiber to the system's input (top-left corner), then collimated and sent to the interferometer (in a thermally-controlled housing, top-right corner). The formed interference fringe pattern is then imaged onto a 16-channel PMT array (bottom-right enclosure) whose outputs (after amplification by a set of trans-impedance amplifiers) are guided to the analog-to-digital converters located in a control and data acquisition computer (not shown here). The setup in Fig. 5b contains a Rasberry-Pi-based local control computer for temperature and setting control (black box in the lower-left corner of the picture).

Another spectrometric receiver version based on a Quadri Mach-Zehnder (QMZ) interferometer is being investigated at ONERA [15]. In this case, the values of four channels arranged in quadrature (non-imaging mode) allow one to determine the Doppler shift. This architecture has the advantage of straightforwardly collecting and analyzing all back-scattered light at once (in the FWFIMI setup, a second back-reflected channel has yet to be added). The measurement is carried out using only four single detectors, which limits the cost and should allow, as for the FWFIMI setup, for good vibration resistance to be obtained: the photosensitive surface being larger than the light spot to be measured, the latter can "move" without affecting the measurement. Recently, the manufacturing of a monolithic version of the QMZ was finalized by the Bertin company. A photo taken during the last alignments is presented in Fig. 6. The monolithic version allows for the elimination of misalignment of the elements of the interferometer, which is extremely critical for its operation.

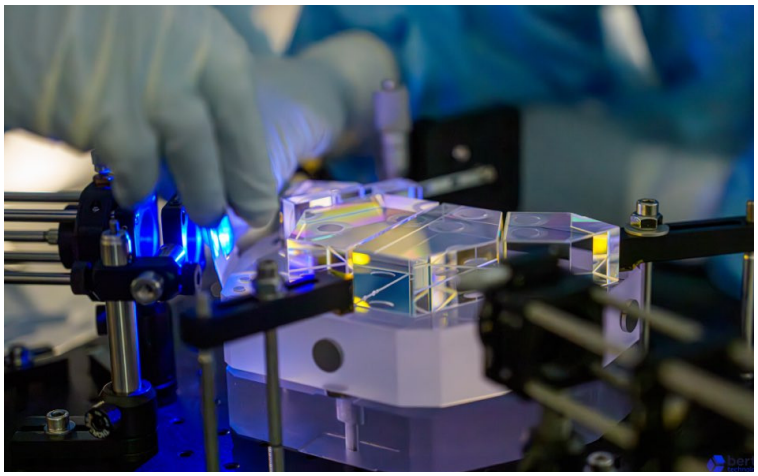

Fig. 6 QMZ interferometer during its final alignment at Bertin (manufacturer). Picture: R. Burla.

D. Wind Reconstruction

For each measurement, the Doppler shift that is determined by the detector corresponds to the so-called line-of-sight velocity, i.e. the relative velocity of the particle or molecules that scattered the light back and the sensor in the direction of the measurement axis. These measurements are not directly usable for gust load alleviation control: several measurements need to be combined to estimate the different wind velocity components. Especially, the variations of the vertical wind velocities are of interest, as they are the main factor driving the maximum gust/turbulence-induced structural loads and fatigue.

To reconstruct the different velocity components based on several line-of-sight measurements, a *wind reconstruction algorithm* (WRA) is needed. Various methods exist for this. The Velocity Azimuth Display (VAD) method was originally developed in the early 1960s to determine the wind velocity and direction with Doppler radars to investigate meteorological phenomena such as precipitation physics and storm dynamics [16]. The method is based on measuring line-of-sight velocities using a scanner with a constant measurement angle $\eta > 0$ (offset w.r.t. the mean measurement direction) rotating at constant speed, thus creating a conical scanning pattern, cf. geometry in Fig. 7. The obtained line-of-sight velocities are then displayed as a function of the scanner azimuth angle ξ for a full cycle of 360°. The original VAD has been improved in numerous ways [17]. VAD is still widely used in context of meteorology [18], atmospheric research [19], and commercial ground-based wind lidars [20]. It is still a common method for feedforward load alleviation of wind turbines (see, e.g., [21, Sect. 4.1] or [22]). However, the VAD is not suitable for aircraft GLA due to several reasons. First, it only works reliably if the wind is sufficiently constant within the scanned volume as shown in [23, Sect. 1]. Secondly, for the GLA application, the aircraft is moving forward at high speed during the lidar scan, so that a circular scan pattern of the lidar causes the measurements to be located along a spiral instead of a circle.

The methods proposed in AWIATOR project ([8, 24, 25])), the INFLIGHT project ([26]), and in the ALFA and MAJESTIC projects ([27]) utilize several discrete measurement axes and can be considered as special cases of the VAD method; hence they share very similar advantages and drawbacks. They have a very short computation time due to their simple measurement geometry using just two (INFLIGHT) or four line-of-sight directions and are guaranteed to obtain a solution within a deterministic time frame. As with the VAD, wind gradients are not accounted for. The aircraft motion within a measurement cycle is not accounted for, at least for the methods used in AWIATOR [8] and ALFA/MAJESTIC method [27]. An interesting contribution of [27] is an analytical investigation of the errors produced by local wind speed variations between the measurement locations – an error source not explicitly taken into account in the AWIATOR approach. Although the effects of such errors in 2-D have long been known and have been described in, e.g., [28, Sect. 4], the proposed 3-D description provides a means to statistically quantify the estimation error for a four-point measurement geometry.

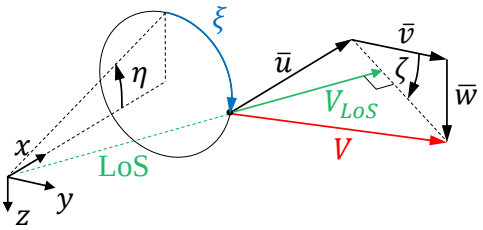

Fig. 7 Velocity azimuth display measurement geometry.

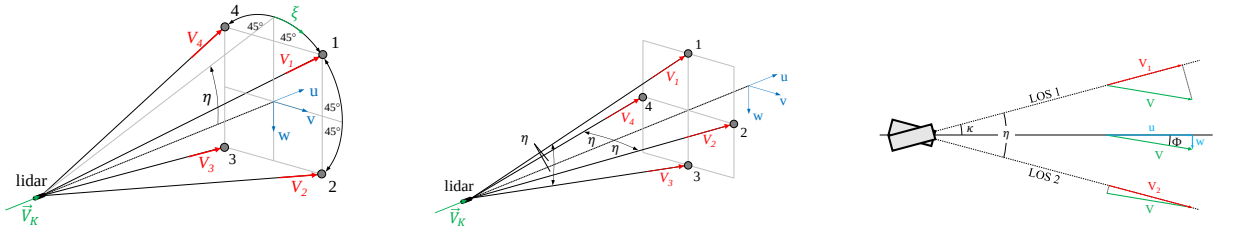

(a) AWIATOR. (b) ALFA/MAJESTIC. (c) INFLIGHT (in aircraft symmetry plane).

Fig. 8 Comparison of the lidar measurement geometries used in the AWIATOR, ALFA/MAJESTIC, and INFLIGHT projects. Each of these cases can be seen as a special case of the VAD geometry of Fig. 7.

Various new or improved wind reconstruction methods are developed in the UP Wing project. One approach from ONERA [29] estimates the six parameters of an arbitrary 1-cosine gust (orientation (three angles), location (intersection on the flight path), gust gradient length, and amplitude) which is immersed in a von Kárman wind field. Based on a four-axis setup, the gust parameters are determined using maximum-likelihood estimation (MLE). It is shown that the gust parameters are reconstructed successfully when the turbulence intensity is negligible compared to the gust

amplitude. By adding a particle filter, more ambiguous estimation problems[‡] are addressed using the capacity of the particle filter to keep track of the different modes of a multi-modal probability density function.

More recently, ONERA also started investigating the use of physics-informed machine learning techniques to reconstruct a 3D turbulence field [30]. In this technique, the "physics-informed" part uses the knowledge/assumption of a von Kárman turbulence model. This work is on-going and at a rather early stage of development, such that the true potential of this wind reconstruction technique is still uncertain at this time.

A wind reconstruction algorithm developed by DLR during the Clean Sky Smart Fixed Wing Aircraft and Clean Sky 2 NACOR projects (cf. [31, 32]): this algorithm is further developed in UP Wing. It accounts for the movement of the aircraft by considering the actual locations and line-of-sight directions at which each of the measurements was taken. By doing so it avoids adding undesired and uncontrolled spatial averaging and distortion of wind gradients[§]. It estimates complete wind profiles instead of making only punctual estimates for a specific location. This provides the option of using spatial regularization which allows reducing the impact of measurement noise with no undesirable phase shifts and also allows for analysis and nonlinear filtering, cf. for instance in [33], to avoid unnecessary actuator activity (and wear) when the turbulence amplitude is small. However, even if its execution time is deterministic, this wind reconstruction method is computationally more demanding than all the previously mentioned methods. To reduce the computational cost of this method, a recursive version was developed. It is also being extended to 2D and 3D grid (from the current 1D wind profiles). The details on these extensions will be published in the near future.

E. Control Design

During the last decade, numerous investigations have been carried out regarding the design of lidar-based gust load alleviation functions [34–43], including the robust tuning and assessment of such controllers. At the start of the UP Wing project, the control design methods were assessed as more mature than the other components (e.g, lidar sensor and wind reconstruction algorithms), so it was decided to focus on further developing those other components while only applying the existing control design methods to the considered aircraft configurations. The load alleviation controllers obtained are coupled with the latest lidar technologies to allow their assessment at aircraft level (cf. Section II.F).

The workflow used to develop the controller is designed for the use of modern, robust controller optimization methods using combinations of H_∞ and H_2 control objectives. It is similar to the process used in [35, Fig. 1] and also leverages the automated process presented in [42]. The lidar-based feedforward controller is integrated with the other controllers using the two-degree-of-freedom structure presented in [43] (cf. Fig. 9). As the lidar-based feedforward controller acts even before the disturbance from the gust/turbulence is measured by the other sensors (e.g., accelerometers and gyros in the IMU or distributed across the airframe), *precompensation* terms are computed and injected on the sensor information used by feedback control functions to prevent them from reacting to (and counteracting) the feedforward controller commands. The need for such precompensation and its effectiveness were demonstrated in [43].

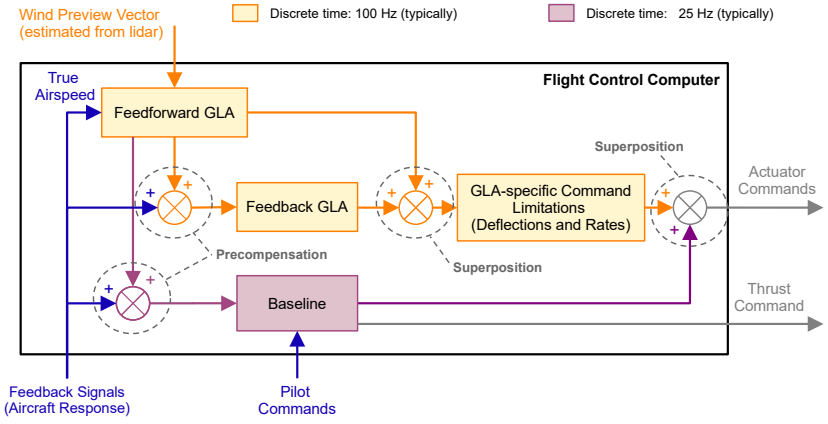

Fig. 9 2-DoF controller structure: internal structure of the flight control functions, simplified version of the diagram presented in [43, Fig. 6].

[‡]i.e., several very different gusts, yet with almost equally good match of the lidar measurements at a given time.

[§]Such averaging and distortion would occur if measurements from different locations are simply mixed together.

F. Aircraft-Level Assessment

For the validation of the results at aircraft-level, a few different aircraft configurations are being considered. In particular, a configuration based on the DLR F25 aircraft configuration (cf. Fig. 10) is used. DLR F25 is a medium-haul aircraft configuration that has been defined to serve as the basis for numerous research projects on climate-compatible flying using innovative technologies. With higher aspect ratio wings, folding wing tips, and in some cases powered with synthetic fuels, DLR-F25-based/derived configurations are among the research configurations distributed by DLR as part of the *Digital Hangar* initiative[¶]. Several variations of DLR-F25 are investigated in the UP Wing project. The *original* version of DLR-F25 is used in the present work.

Fig. 10 Three-dimensional view of the DLR-F25 concept[‖] – Credit: DLR (CC BY-NC-ND 3.0).

The overall performance of the designed lidar-based load alleviation system is assessed on a multi-rate hybrid simulation environment (see Fig. 11) built around the considered aircraft configurations (DLR F25 and another configuration from an industry partner). In this environment, a surrogate model of the lidar sensor is used (simplified stochastic model of the lidar instrument, which is an evolution of the model described in [11]) and coupled with the wind reconstruction algorithm and the different controller functions. Electromechanical actuators are used to actuate all different control surfaces: the actuators considered are based on those presented in [44, 45].

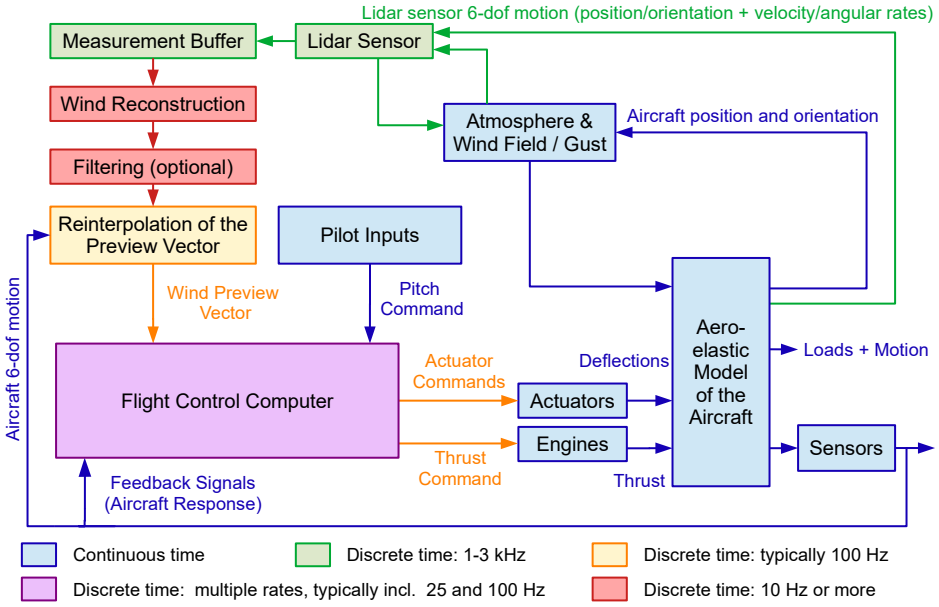

Fig. 11 Multi-rate hybrid simulation used for aircraft-level assessment of lidar-based GLA systems.

[¶]see https://digital-hangar.de/

[‖]cf. https://www.dlr.de/en/latest/news/2025/explore-next-generation-aircraft-in-the-digital-hangar/dlr-f25-concept

III. Overview of the Main Demonstrations

This section presents the main demonstrations that are conducted in UP Wing on the lidar-based GLA topic: the lab and integration tests are presented in Section III.A, the ground-based altitude tests Section III.B, and finally the flight tests in Section III.C.

A. Lab and Integration Tests

For a basic functionality test, the most important parameters of the DLR laser were validated before lab tests together with the receiver system were performed.

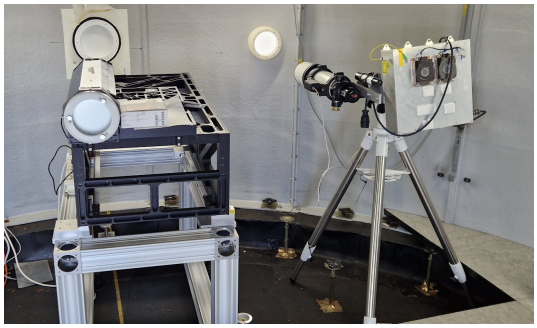

(a) Racks with windows to the outside of the dome.

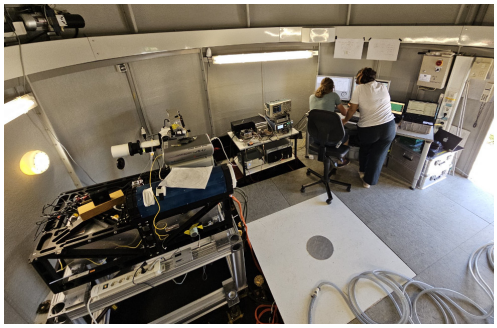

(b) Inside the dome on the roof of the building, during tests.

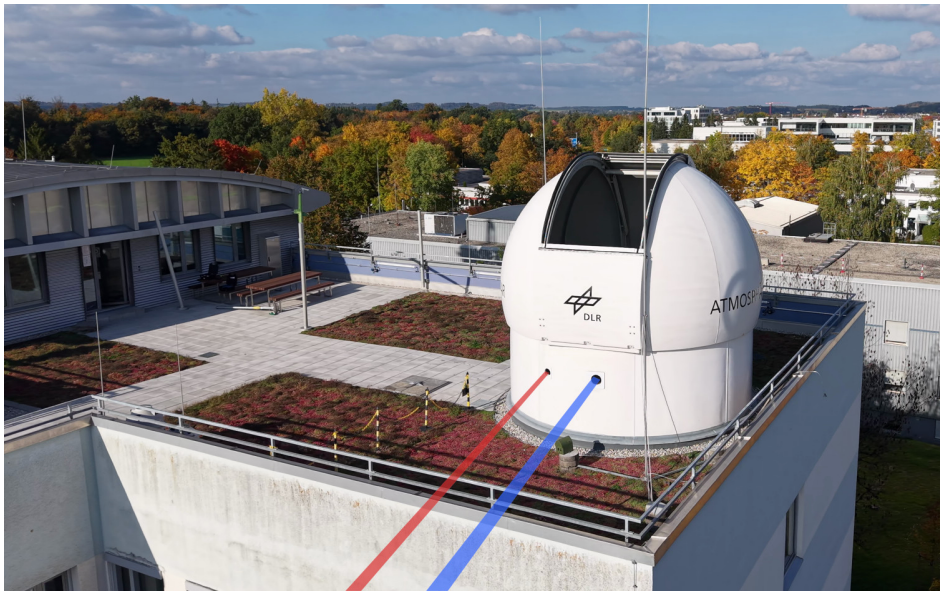

(c) Outside view of the dome with indicated lidar beams (blue for the developed direct-detection ultraviolet lidar, red for coherent infrared lidar when used for comparison).

Fig. 12 Lab and ground tests at DLR's Oberpfaffenhofen site (near Munich).

The lidar was installed in the lidar dome on top of the atmospheric physics department building at DLR Oberpfaffenhofen to obtain atmospheric signal, see Fig. 12. For the laser and telescope, the rack system that will be used for the flight tests was already used for these ground tests. These tests included investigation of output power requirements, pulse energy jitter, availability of a reference signal, communication between the laser and the newly developed data acquisition unit, and GPS-based time synchronization. Furthermore, an envelope for suitable laser operating points was identified and minor bugs or issues with the hardware and software were fixed. The data evaluation software was optimized for new data formats and a slightly different workflow. In the course of these overall system tests, some optimization opportunities with the laser source, like longer-term optical damage and laser frequency instabilities, were identified and have already been or are currently being addressed.

B. Ground-Based Altitude Tests

As an intermediate step between laboratory tests and flight tests, high-altitude lidar ground tests are planned for Q1/Q2 2026 together with the newly developed DLR laser source and the new ONERA system. Before the UP Wing project, high-altitude ground tests of the DLR receiver were successfully performed using an alternative laser source that was originally built and optimized for a different application [46]. This time, prototypes optimized for the need of the gust load alleviation application will be tested.

The selected location is the Bavarian State's Environmental Research Station *UFS Schneefernerhaus*[**], just below the summit of the mount Zugspitze at the German-Austrian border near the town of Garmisch-Partenkirchen, cf. Fig. 13.

Fig. 13 Front view of the UFS Schneefernerhaus, Picture: UFS GmbH, CC BY-SA 4.0, via Wikimedia Commons.

Originally built in 1931 as a hotel, it has been an environmental research station since 1999. It is located at about 2650 m (8700 ft) MSL. This altitude is far from modern aircraft cruise altitudes, but represents a good compromise between more representative atmospheric conditions (often with very low aerosol concentrations) and accessibility with the required equipment. Contrary to flight tests, the equipment does not need to be qualified and it is possible to work on, modify, and operate the system for days or weeks, while living in the station. As for low-altitude ground test, it is possible to use other sensors as truth-tellers, such as a 3D ultra-sonic anemometer at the top of the next mountain peak, a coherent lidar sensor when the aerosol concentration is sufficient, and further environmental-monitoring devices (such as aerosol particle quantification equipment) of the German Federal Environment Agency (UBA) and the German Weather Service (DWD).

C. Flight Tests

A flight test campaign with the NLR Cessna Citation II is planned for August 2026. This aircraft had already been used in a previous European project called DELICAT[††] in which a different type of forward looking lidar sensor was developed and tested in flight [4–6]. For the purpose of the flight test in the UP Wing project, some of the aircraft modifications developed and qualified for the DELICAT project can be reused, which makes this test aircraft particularly advantageous for these tests. Figure 14 shows the aircraft with the air data boom that will provide reference air data measurements.

Following a trial installation of the air data boom, a first flight was performed on April 9th, 2025 over the North Sea, off the coast of the Netherlands, to test the boom and gather the required data for its calibration, cf. Fig. 15.
The three main objectives for the lidar flight test campaign in August 2026 are:

1) validate the lidar's ability of uni-axial wind speed measurement performance in aerosol-devoid air,
2) validate the lidar performance through direct comparison with the reference air data system mounted on the air data boom (i.e., primarily wind speed), and
3) characterize the response of the sensor to turbulent wind.

[**]https://schneefernerhaus.de/en/

[††]funded within the Framework Programme 7 of the European Community for research, technological developments, and demonstration activities

(a) On ground during the installation of the air data boom on the aircraft nose.

(b) Close up pictures of the air data boom.

Fig. 14 NLR Cessna Citation II (PH-LAB) with its Air Data Boom.

To achieve these objectives, various atmospheric conditions are desirable. Based on aerosol and turbulence climatology and also due to the low air traffic (organization with national ATC), the region of Trondheim, Norway has been selected and it is planned to use Trondheim's Airport (ICAO code ENVA) as base location during the test campaign. This region offers good access to both windward / oceanic clean air and leeward (Jotunheimen mountains) with possible mountain wave and turbulence events.

For day-to-day flight planning, DLR has set up tools and will provide on-site meteorological forecasters to give a daily morning briefing, allowing for efficient and optimized flight planning by the scientists operating the lidar systems and the NLR test pilots. On the server of the DLR Institute of Atmospheric Physics, an adapted domain will provide the latest ECMWF IFS forecast with special products such as Eddy Dissipation Rate (EDR) twice a day. DLR also provides its Mission Support Tool / MSS that gathers all necessary meteorology and plan flight tracks (exporting series of flight points) in a few synthetic views. A selection of typical forecast diagrams is shown in Fig. 16.

To allow the analysis of the lidar performance, the atmospheric conditions must be known. The aircraft is equipped with sensors that already measure factors such as pressure and temperature. An essential parameter for a lidar sensor is also the presence of aerosols: DLR adapted a highly compact commercial particle size spectrometer (aimed at balloon-borne operation) to the low pressure conditions encountered at high altitude by placing it into a pressure-tight vessel and adding a pump. This Aerosol Particle Spectrometer Assembly (APSA) device (cf. Fig. 17a) is connected to the input and return tubes of a skin panel (cf. Fig. 17b) that NLR developed to contribute to the volcanic dust observations campaigns that took place during the famous Eyyafjalla eruption in 2010.

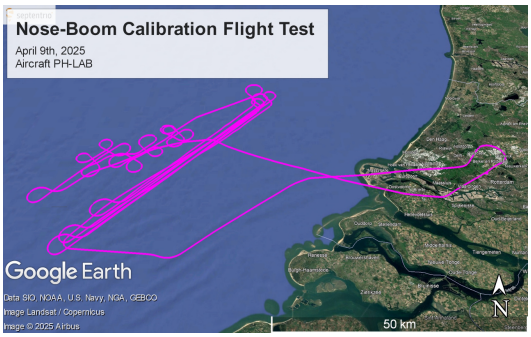

(a) Ground track of the flight used for calibrating the air-data boom (see copyright in the bottom-left corner).

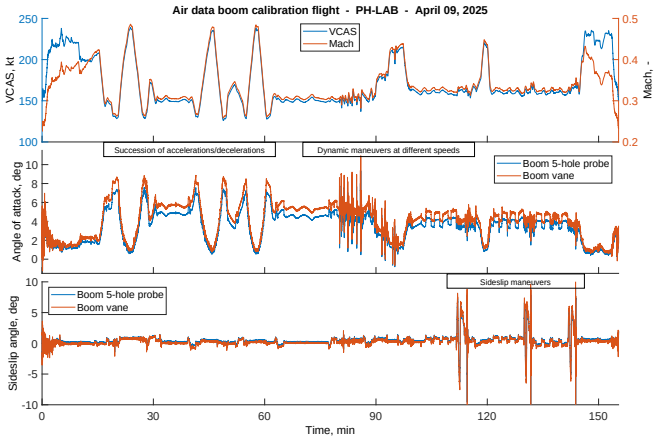

(b) Illustration of the maneuvers and data for the calibration.

Fig. 15 Ground track and raw signals for air data boom sensor calibration.

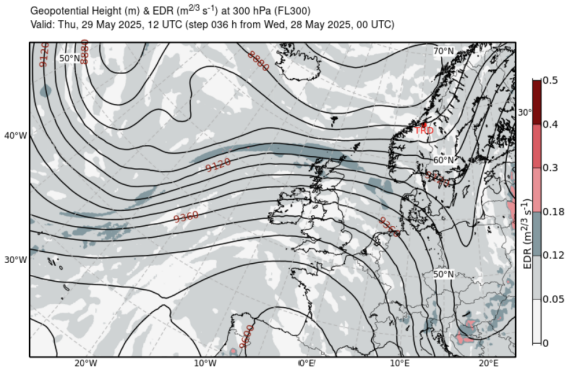

(a) Eddy Dissipation Rate (EDR) at specific altitude level issued from the European Centre for Medium-Range Weather Forecasts (ECMWF) IFS forecast by DLR Institute of Atmospheric Physics' Mission Support website.

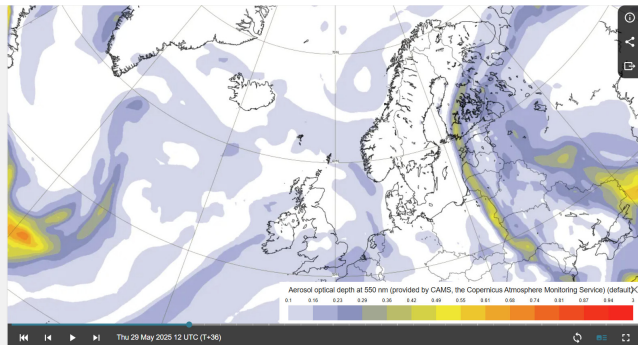

(b) Aerosol optical depth at 550 nm from the CAMS model (Copernicus Atmosphere Monitoring Service), implemented by ECMWF [47].

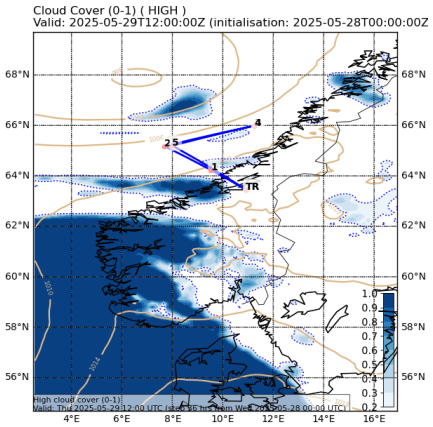

(c) Cloud cover map, issued from the Mission Support Service tool [48].

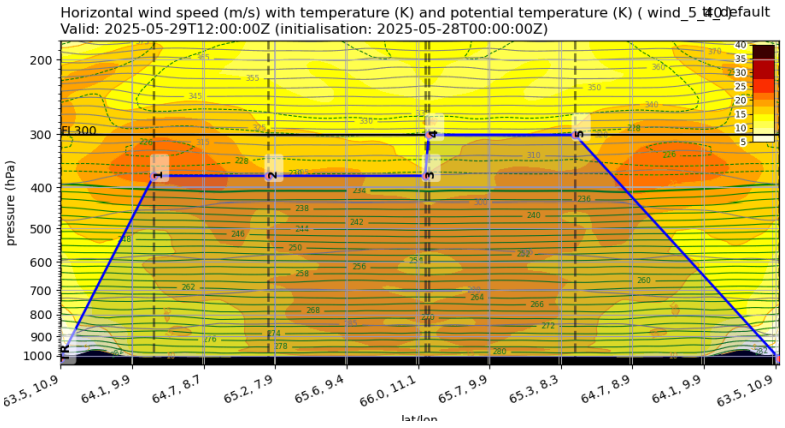

(d) Vertical slice along a aircraft trajectory, planned and depicted by the Mission Support Service tool [48].

Fig. 16 View of different meteorological forecasting tools to support the day-to-day flight planning during the flight test campaign.

http://arc.aiaa.org | DOI: 10.2514/6.2026-1383

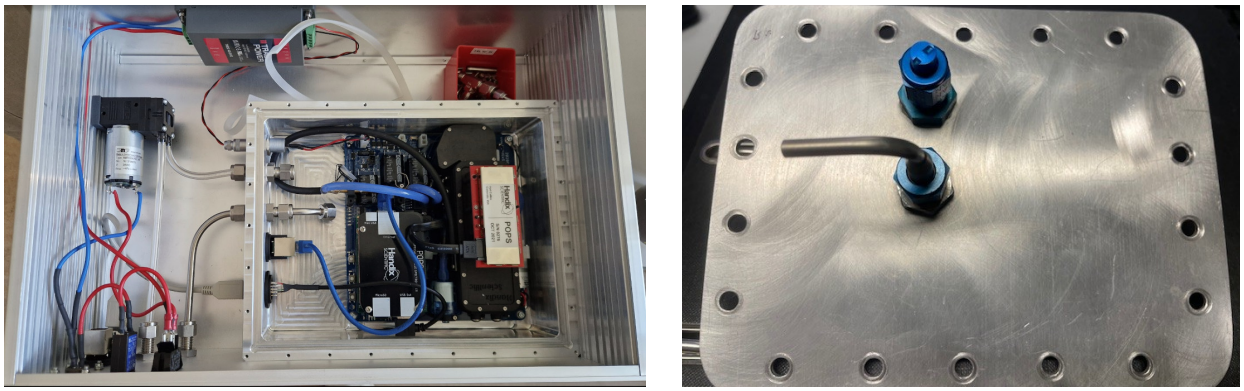

(a) Aerosol Particle Spectrometer Assembly (APSA) based on the commercial Handix Scientific Inc. POPS instrument.

(b) NLR's inlet skin panel allowing to probe the ambient air.

Fig. 17 Equipment for characterizing the current atmospheric conditions.

IV. Conclusion

Numerous technological developments covering all aspects of a complete lidar-based gust load alleviation system were presented. The progress and current status on these developments and the demonstration activities are on track for the major demonstration activities planned this year (2026), first with the high-altitude ground tests Q1-Q2/2026 and the flight tests around August 2026. The results of these tests will be published soon after.

Acknowledgments

This work is part of the Ultra Performance Wing (UP Wing, project number: 101101974) project, which is supported by the Clean Aviation Joint Undertaking and its members.

The ONERA authors would like to thank Romain Burla from the Bertin company for the picture shown in Fig. 6. The ONERA authors also would like to thank their project co-worker T. Boulant, L. Bizet, J. Gauthier, D. Goular, J. Houy, L. Lombard, C. Planchat, M. Valla, F. De La Barrière, Y. Ferrec, O. Gazzano, P. Perrault, E. Lambert, R. Domel, S. Lefebvre, F. Dambreville, A. Capmas-Pernet from ONERA, J. F. Mariscal, N. Rouanet from the LATMOS laboratory and Pascal Huguet-Chantome from the Bertin company for their extensive support.

The DLR authors warmly thank their project co-workers Paula Cutipa, Matteo Faccioni, Oliver Kleinert, Adithya Pankan, Christian Wallace, Davide Cavaliere, Matthias Damm, Oliver Kliebisch, Peter Mahnke, Gerhard Geyer, as well as the further colleagues Tanja Bodenbach, Bernd Kaifler, Markus Pinzer, Daniel Sauer for their support.

The NLR authors warmly thank their colleagues Anna Biancotto, Thomas Dumoulin, and Huib Schriemer.

Disclaimer

Co-Funded by the European Union. Views and opinions expressed are however those of the author(s) only and do not necessarily reflect those of the European Union or Clean Aviation Joint Undertaking. Neither the European Union nor the granting authority can be held responsible for them.

Co-funded by the European Union

References

[1] Matthes, S., Lim, L., Burkhardt, U., Dahlmann, K., Dietmüller, S., Grewe, V., Haslerud, A. S., Hendricks, J., Owen, B., Pitari, G., Righi, M., and Skowron, A., "Mitigation of Non-CO2 Aviation's Climate Impact by Changing Cruise Altitudes," *Aerospace*, Vol. 8, No. 2, 2021. https://doi.org/10.3390/aerospace8020036, URL https://www.mdpi.com/2226-4310/8/2/36.

[2] Eberle, A., Stefes, B., and Reckzeh, D., "Clean Aviation Ultra-Performance Wing (UP-Wing)," *AIAA SCITECH 2024 Forum*, 2024. https://doi.org/10.2514/6.2024-2109.

[3] Fezans, N., Vrancken, P., Linsmayer, P., Wallace, C., and Deiler, C., "Designing and Maturating Doppler Lidar Sensors for Gust Load Alleviation: Progress Made Since AWIATOR," *Proceedings of the Aerospace Europe Conference*, CEAS / 3AF, Bordeaux, France, 2020. https://doi.org/10.60801/aec2020-556.

[4] Vrancken, P., Wirth, M., Ehret, G., Barny, H., Rondeau, P., and Veerman, H., "Airborne forward-pointing UV Rayleigh lidar for remote clear air turbulence detection: system design and performance," *Appl. Opt.*, Vol. 55, No. 32, 2016, pp. 9314–9328. https://doi.org/10.1364/AO.55.009314, URL https://opg.optica.org/ao/abstract.cfm?URI=ao-55-32-9314.

[5] Veermann, H., Vrancken, P., and Lombard, L., "Flight testing DELICAT – A promise for medium-range Clear Air Turbulence protection," *46th SETP Symposium and 25th SFTE Symposium*, 2014. URL https://elib.dlr.de/91968/.

[6] Vrancken, P., Wirth, M., Ehret, G., Witschas, B., Veermann, H., Tump, R., Barny, H., Rondeau, P., Dolfi-Bouteyre, A., and Lombard, L., "Flight Tests of the DELICAT Airborne LIDAR System for Remote Clear Air Turbulence Detection," *EPJ Web of Conferences*, The 27th International Laser Radar Conference (ILRC 27), Vol. 119, 2015. URL https://elib.dlr.de/123548/.

[7] Schmitt, N. P., Rehm, W., Pistner, T., Zeller, P., Diehl, H., and Navé, P., "The AWIATOR airborne LIDAR turbulence sensor," *Aerospace Science and Technology*, Vol. 11, 2007, pp. 546–552. https://doi.org/10.2514/1.44950.

[8] Jenaro Rabadan, G., Schmitt, N. P., Pistner, T., and Rehm, W., "Airborne lidar for automatic feedforward control of turbulent in-flight phenomena," *Journal of Aircraft*, Vol. 47, No. 2, 2010, pp. 392–403. https://doi.org/10.2514/1.44950.

[9] Illingworth, J., and Kittler, J., "The Adaptive Hough Transform," *IEEE Transactions on Pattern Analysis and Machine Intelligence*, Vol. PAMI-9, No. 5, 1987, pp. 690–698. https://doi.org/10.1109/TPAMI.1987.4767964.

[10] Vrancken, P., Bizet, L., Boulant, T., Cutipa, P., Fezans, N., Faccioni, M., de Haan, H., Jentink, H., Kiehn, D., Kliebisch, O., Linsmayer, P., Lombard, L., Lorbeer, R.-A., Michel, D. T., Pichon, P., Pouillaude, J., Pankan, A. S., Thurn, J., Tump, R., and Valla, M., "Aeronautics lidar revisited - Towards lidar-based gust and turbulence measurement for aircraft load alleviation control," *31st International Laser Radar Conference (ILRC)*, edited by A. Fix, EPJ Web of Conferences, 2024, pp. 1–4. URL https://elib.dlr.de/205242/.

[11] Vrancken, P., and Herbst, J., "Aeronautics Application of Direct-Detection Doppler Wind Lidar: An Adapted Design Based on a Fringe-Imaging Michelson Interferometer as Spectral Analyzer," *Remote Sensing*, Vol. 14, 2022. https://doi.org/10.3390/rs14143356.

[12] Herbst, J., and Vrancken, P., "Design of a monolithic Michelson interferometer for fringe imaging in a near-field, UV, direct-detection Doppler wind lidar," *Applied Optics*, Vol. 55, No. 25, 2016, pp. 6910–6929. https://doi.org/10.1364/AO.55.006910.

[13] Herbst, J., "Development and test of a UV lidar receiver for the measurement of wind velocities aiming at the near-range characterization of wake vortices and gusts in clear air," Phd thesis, Ludwig-Maximilian University, Munich, Germany, April 2019. https://doi.org/10.5282/edoc.24347.

[14] Linsmayer, P., and Vrancken, P., "Windspeed determination from a near-field, UV, direct-detection Doppler wind lidar based on Michelson interferometer fringe imaging," *Applied Optics*, Vol. 64, No. 8, 2025, pp. 1745–1756. https://doi.org/10.1364/AO.546163.

[15] Boulant, T., Bizet, L., Valla, M., Gazzano, Y. F., and Michel, T., "Direct-detection airborne UV wind lidar including Quadri Mach-Zehnder interferometer for 3D wind reconstruction," *Proceedings of the 2024 Coherent Laser Radar Conference (CLRC)*, Landshut, Germany, 2024. URL https://hal.science/hal-04714604/.

[16] Probert-Jones, J. R., "Meteorological use of pulsed Doppler radar," *Nature*, Vol. 186, No. 4721, 1960, pp. 271–273.

[17] Liu, Z., Barlow, J. F., Chan, P.-W., Fung, J. C. H., Li, Y., Ren, C., Mak, H. W. L., and Ng, E., "A Review of Progress and Applications of Pulsed Doppler Wind LiDARs," *Remote Sensing*, Vol. 11, No. 21, 2019. https://doi.org/10.3390/rs11212522.

[18] Baidar, S., Wagner, T. J., Turner, D. D., and Brewer, W. A., "Using optimal estimation to retrieve winds from velocity-azimuth display (VAD) scans by a Doppler lidar," *Atmospheric Measurement Techniques*, Vol. 16, No. 15, 2023, pp. 3715–3726. https://doi.org/10.5194/amt-16-3715-2023.

[19] Chouza, F., Reitebuch, O., Jähn, M., Rahm, S., and Weinzierl, B., "Vertical wind retrieved by airborne lidar and analysis of island induced gravity waves in combination with numerical models and in situ particle measurements," *Atmospheric Chemistry and Physics*, Vol. 16, No. 7, 2016, pp. 4675–4692. https://doi.org/10.5194/acp-16-4675-2016.

[20] Stephan, A., Wildmann, N., and Smalikho, I. N., "Effectiveness of the MFAS Method for Determining the Wind Velocity Vector from Windcube 200s Lidar Measurements," *Atmospheric and Oceanic Optics*, Vol. 32, 2019, p. 555–563. https://doi.org/10.1134/S1024856019050166.

[21] Kapp, S., "Lidar-based Reconstruction of Wind Fields and Application for Wind Turbine Control," Ph.D. thesis, Universität Oldenburg, 2017. URL https://oops.uni-oldenburg.de/id/eprint/3210.

[22] Wildmann, N., Thayer, J. D., Detring, C., and Päschke, E., "Gust-detection from velocity azimuth display Doppler wind lidar profiling at the WiValdi research park," *Journal of Physics: Conference Series*, Vol. 2767, No. 9, 2024, p. 092076. https://doi.org/10.1088/1742-6596/2767/9/092.

[23] Caya, D., and Zawadzki, I., "VAD Analysis of Nonlinear Wind Fields," *Journal of Atmospheric and Oceanic Technology*, Vol. 9, No. 5, 1992, pp. 575 – 587. https://doi.org/10.1175/1520-0426(1992)009<0575:VAONWF>2.0.CO;2.

[24] Schmitt, N. P., Rehm, W., Pistner, T., Zeller, P., Diehl, H., and Navé, P., "Airborne direct detection UV lidar," *Proceedings of 23rd International Laser Radar Conference (ILRC)*, 2006, pp. 167–170.

[25] Schmitt, N. P., Rehm, W., Pistner, T., Diehl, H., Navé, P., Jenaro-Rabadan, G., Mirand, P., and Reymond, M., "Forward Looking Clear Air Turbulence Measurement with the AWIATOR LIDAR Sensor," *Proceedings of the 1st CEAS European Air and Space Conference*, Berlin, Germany, 2007, pp. 179–184. CEAS-2007-204.

[26] Sandvoß, C.-S., and Steen, M. E., "Abschlussbericht INFLIGHT– Innovative Flugregelung und echtzeitfähige LIDAR onboard Messtechnik für leichtere, komfortablere Flugzeuge," Tech. rep., Technische Universität Braunschweig, Institut für Flugführung, Mar. 2022.

[27] Boulant, T., Michel, T., and Valla, M., "Optimization of a direct detection UV wind lidar architecture for 3D wind reconstruction at high altitude," *Atmospheric Measurement Techniques Discussions*, Vol. 2024, 2024, pp. 1–19. https://doi.org/10.5194/amt-2024-41.

[28] Soreide, D. C., Bogue, R. K., Ehernberger, L., and Bagley, H. R., "Coherent lidar turbulence measurement for gust load alleviation," *Optical instruments for weather forecasting*, Vol. 2832, SPIE, 1996, pp. 61–75.

[29] Musso, C., Boulant, T., Valla, M., Lefebvre, S., and Michel, D.-T., "Estimation of the Parameters of a Three-Dimensional Gust Model with a Wind Lidar," *AIAA Journal*, Vol. 0, No. 0, 0, pp. 1–12. https://doi.org/10.2514/1.J064209.

[30] Capmas-Pernet, A., Musso, C., Dambreville, F., Valla, M., and Michel, T., "Physics-informed machine learning for reconstruction of wind turbulence with wind lidar," *Proceedings of the 11th International Conference on Machine Learning, Optimization, and Data Science*, Riva del Sole, Italy, 2025.

[31] Fezans, N., Schwithal, J., and Fischenberg, D., "In-flight remote sensing and identification of gust, turbulence, and wake vortices using a Doppler LIDAR," *CEAS Aeronautical Journal*, Vol. 8, No. 2, 2017, pp. 313–333. https://doi.org/10.1007/s13272-017-0240-9.

[32] Fezans, N., Joos, H.-D., and Deiler, C., "Gust load alleviation for a long-range aircraft with and without anticipation," *CEAS Aeronautical Journal*, Vol. 10, No. 4, 2019, pp. 1033–1057. https://doi.org/10.1007/s13272-019-00362-9.

[33] Fezans, N., *An Unusual Structure for a Feedforward Gust Load Alleviation Controller*, Advances in Aerospace Guidance, Navigation and Control, Springer-Verlag Berlin Heidelberg, 2017, pp. 47–68. https://doi.org/10.1007/978-3-319-65283-2.

[34] Fournier, H., Massioni, P., Pham, M. T., Bako, L., Vernay, R., and Colombo, M., *Robust Gust Load Alleviation at Different Flight Points and Mass configurations*, ???? https://doi.org/10.2514/6.2022-0285.

[35] Fezans, N., Wallace, C., Kiehn, D., Cavaliere, D., and Vrancken, P., "Lidar-Based Gust Load Alleviation - Results Obtained on the Clean Sky 2 Load Alleviation Benchmark," *Proceedings of the 19th International Forum on Aeroelasticity and Structural Dynamics (IFASD) 2022*, Vol. 4, 2022, pp. 2010–2038. https://doi.org/10.60801/IFASD-2022-155.

[36] Cavaliere, D., Fezans, N., and Kiehn, D., "Method to Account for Estimator-Induced Previewed Information Losses – Application to Synthesis of Lidar-Based Gust Load Alleviation Functions," *CEAS EuroGNC 2022, May 3–5 2022, Berlin, Germany*, 2022.

[37] Wallace, C., Schulz, S., Fezans, N., Kier, T., and Weber, G., "Evaluation Environment for Cascaded and Partly Decentralized Multi-Rate Load Alleviation Controllers," *33rd Congress of the International Council of the Aeronautical Sciences (ICAS)*, 2022. https://doi.org/10.60801/ICAS-2022-0656.

[38] Fournier, H., Massioni, P., Tu Pham, M., Bako, L., Vernay, R., and Colombo, M., "Robust Gust Load Alleviation of Flexible Aircraft Equipped with Lidar," *Journal of Guidance, Control, and Dynamics*, Vol. 45, No. 1, 2022, pp. 58–72. https://doi.org/10.2514/1.G006084.

[39] Wallace, C., and Fezans, N., "Lidar-based Gust Load Alleviation - Results Obtained on a Generic Long Range Aircraft Configuration," *CEAS – EUCASS Aerospace Europe Conference 2023*, 2023. https://doi.org/10.13009/EUCASS2023-564.

[40] Cavaliere, D., Fezans, N., Kiehn, D., Schultz, J., and Römer, U., "Linear Modeling of Doppler Wind Lidar Systems for Gust Load Alleviation Design," *Journal of Guidance, Control, and Dynamics*, Vol. 47, No. 11, 2024, pp. 2351–2368. https://doi.org/10.2514/1.G008040.

[41] Cavaliere, D., and Fezans, N., "Toward Automated Gust Load Alleviation Control Design via Discrete Gust Impulse Filters," *Journal of Guidance, Control, and Dynamics*, Vol. 47, No. 4, 2024, pp. 697–710. https://doi.org/10.2514/1.G007762.

[42] Cavaliere, D., and Fezans, N., "A Practical Approach to Automated Multiobjective Gust Load Alleviation Control Design in a Structured H_2/H_∞ Framework," *Proceedings of the 2024 CEAS EuroGNC conference*, Bristol, UK, 2024. https://doi.org/10.82124/CEAS-GNC-2024-042.

[43] Wallace, C., and Fezans, N., "Lidar-based gust load alleviation -– increasing the load reduction potential through a two-degree-of-freedom controller architecture," *Proceedings of the 2024 IFASD Conference*, The Hague, The Netherlands, 2024. IFASD-2024-163.

[44] Kowalski, R., and Juchmann, P., "Sensorless motor control for electro-mechanical flight control actuators," *CEAS Aeronautical Journal*, 2023. https://doi.org/10.1007/s13272-023-00682-x.

[45] Kowalski, R., "Drehgeberlose Regelung elektromechanischer Flugsteuerungsaktuatoren," Ph.D. thesis, 2024. https://doi.org/10.57676/hcb3-9c65.

[46] Wirth, M., Fix, A., Mahnke, P., Schwarzer, H., Schrandt, F., and Ehret, G., "The airborne multi-wavelength water vapor differential absorption lidar WALES: system design and performance," *Applied Physics B*, Vol. 96, No. 1, 2009, p. 201. https://doi.org/10.1007/s00340-009-3365-7.

[47] Copernicus - the European Union's Earth observation programme, "CAMS: Copernicus Atmosphere Monitoring Service - Aerosol forecasts," , (accessed in May. 2025). URL https://atmosphere.copernicus.eu/charts/packages/cams/products/aerosol-forecasts.

[48] Rautenhaus, M., Bauer, G., and Dörnbrack, A., "A web service based tool to plan atmospheric research flights," *Geoscientific Model Development*, Vol. 5, No. 1, 2012, pp. 55–71. https://doi.org/10.5194/gmd-5-55-2012, URL https://gmd.copernicus.org/articles/5/55/2012/.